Hindawi
Geofluids
Volume 2022, Article ID 4681189, 13 pages
https://doi.org/10.1155/2022/4681189

Research Article

Flow Field Simulation of Swirling Abrasive Jet Nozzle for Hard Rock Breaking

Zhang Dongqing,[1] Li Jingbin,[2] Hu Xiao,[2] Liu Xin,[2] and Cheng Kang[2]

[1]*State Key Laboratory of Shale Oil and Gas Enrichment Mechanisms and Effective Development, Beijing 102249, China*
[2]*China University of Petroleum Beijing, Beijing 102249, China*

Correspondence should be addressed to Li Jingbin; lijb@cup.edu.cn

Received 31 December 2021; Revised 25 January 2022; Accepted 14 February 2022; Published 9 March 2022

Academic Editor: Afshin Davarpanah

Radial jet drilling (RJD) technology has been proved to be an economical and efficient stimulation technology for oil and gas, geothermal, hydrate, etc. but conventional RJD technology adopts pure water jet to break rock and form laterals, which has low rock breaking efficiency and is unable to effectively break hard rock such as shale. Swirling abrasive jet is proposed to promote the development of RJD. Here, the characteristics of the flow field of the swirling abrasive jet nozzle and the influence of the key impeller parameters are studied by numerical simulation. The distribution and development of axial velocity, tangential velocity, and radial velocity of water and abrasive are analyzed. The results show that the swirling abrasive jet has no constant velocity core, has stronger diffusivity, and can form a larger impact area than the direct jet. Abrasive particles and water can acquire large tangential and radial velocity which can break rock under the action of shear and tensile stress efficiently. With the increase of the spinning angle, the axial velocity of the fluid decreases, and the tangential velocity increases gradually. With the increase of blade thickness, the axial velocity decreases, and the tangential velocity increases. With the increase of the number of blades, the axial velocity decreases, and the tangential velocity increases. The spinning direction almost has no effect on the flow field. Therefore, the spinning angle is recommended to be no less than 270°, blade thickness is 2.5 mm, and number of blades are 3. The research results provide theoretical guidance for the structural design of swirling abrasive jet nozzles.

1. Introduction

Radial jet drilling (RJD) technology can drill one or more horizontal laterals, whose diameter is about 30~50 mm and the maximum length is about 100 m, along the radial direction perpendicular to the main wellbore by hydraulic jetting. Multiple operations can form a three-dimensional well pattern structure of "multiple layers in one well and multiple branches in the same layer" [1–4]. RJD technology can increase the contact area with reservoir, establish high diversion channel, and efficiently exploit complex oil and gas reservoirs, which has achieved good application. Combined with reservoir simulation technologies such as hydraulic fracturing, full three-dimensional reconstruction can be realized to achieve the goal of enhanced oil recovery [5–13]. Recently, with more and more attention paid to clean energy, RJD technology is considered as an effective geothermal and hydrate resource development technique [14–17].

However, conventional RJD technology adopts pure water jet to break rock and form laterals. The high-pressure water jet technology is the key technology of RJD. Scholars have developed multiorifice nozzle [18, 19], swirling nozzle [20], and straight-swirling integrated nozzle [21] to achieve efficient rock breaking, but pure water jet has low rock breaking efficiency and is unable to effectively break granite, shale, carbonate, and other hard rocks. Therefore, it is necessary to develop new efficient rock breaking technology to promote the development and application of RJD technology.

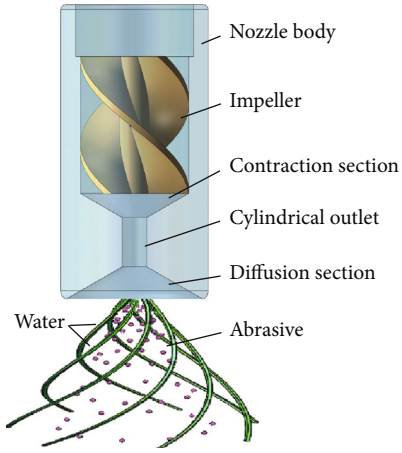

Figure 1: Structure diagram of swirling abrasive jet nozzle.

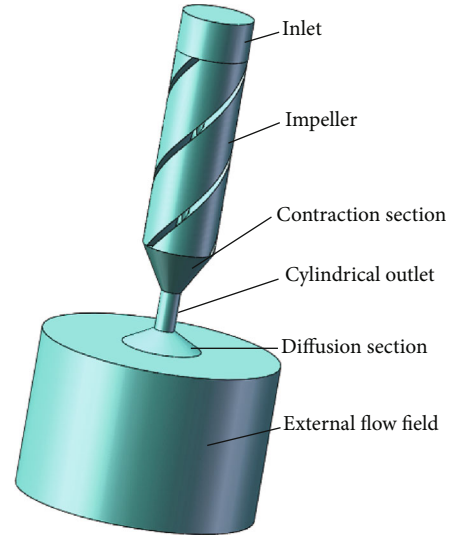

Figure 2: Physical model of swirling abrasive jet nozzle.

Abrasive water jet (AWJ) technology, which is a liquid-solid two-phase jet formed by adding solid particles (garnet or quartz sand, etc.) into high-speed flowing water, is used for a wide range of industrial applications, mainly for cutting and surface treatment [22]. Due to the impact and cutting action of abrasive particles, AWJ has much better rock-breaking performance [23]. AWJ is widely used in petroleum engineering, such as casing cutting, perforating, and hydraulic jet fracturing [24–27]. Huang et al. [28] verified that the abrasive jet has much higher rock-breaking ability. Niu et al. [29] optimized the jet parameters and abrasive parameters in the process of hydraulic jet fracturing through experimental methods. Under the experimental conditions, there is an optimal abrasive volume fraction (6%-8%) and an optimal abrasive particle size range (0.4-0.6 mm).

Although abrasive jet has strong rock breaking ability and high rock breaking efficiency, it has poor diffusivity and only forms small diameter rock-breaking hole, which cannot meet the demand of subsequent pipeline entering the formation. Therefore, Yang et al. [30] proposed swirling abrasive jet technology, which combined the characteristics of abrasive jet and swirling jet. A spiral impeller is added into the classic conical nozzle, so that the fluid and abrasive can obtain high radial and tangential velocity and then form a large impact diameter. Compared with the traditional direct jet, swirling abrasive jet shows complex and unique flow characteristics. Therefore, here, the flow field characteristics of swirling abrasive jet are studied by numerical simulation. Influence of impeller parameters on the flow field is analyzed. The research results can provide guidance for structural optimization design of swirling abrasive jet nozzle.

2. Structure and Principle of Swirling Abrasive Jet Nozzle

As shown in Figure 1, the swirling abrasive jet nozzle is mainly composed of the nozzle body, the impeller, the contraction section, the cylindrical outlet, and the diffusion section. High pressure water and abrasive are bumped to the nozzle by high-pressure plunger pump, through and swirl under the guidance of the impeller, obtain a higher velocity due to the decrease of the cross-sectional area of the contraction section, and then are jetted from the cylinder outlet. Under the protection of the diffusion section, a fully developed swirling abrasive jet is formed. The fluid acquires higher axial, tangential, and radial velocities, and the abrasive also achieves a higher three-dimensional velocity under the action of fluid carrying and acceleration. The rock breaking efficiency of abrasive jet is much higher than that of pure water jet [20]; so, the swirling abrasive jet can effectively break most rocks, even limestone, granite, etc. In addition, because the swirling abrasive jet has higher tangential and radial velocity, the fully developed swirling abrasive jet can form a large diameter hole. The swirling abrasive jet can efficiently break rocks and form large diameter radial branches, which is very suitable for RJD technology.

3. Numerical Simulation Model

3.1. Physical Model and Control Equation

3.1.1. Physical Model. The physical model of the swirling abrasive nozzle is shown as Figure 2. The main composition and basic parameters of the model are as follows: the nozzle inlet with 18 mm diameter, the impeller with 50 mm length, the contraction section with 60° angle, the cylinder outlet with 5 mm diameter and 10 mm length, the diffusion section with 120°angle, and the impact external flow field which is a cylinder with 40 mm height and 60 mm diameter.

3.1.2. Governing Equation. The turbulent viscosity model will directly affect the accuracy of the calculation results. The standard k-epsilon model is a two-equation model in the typical RANS vortex viscosity model. This model is a widely used turbulence model at present. It has a relatively simple calculation format, and better results can be obtained.

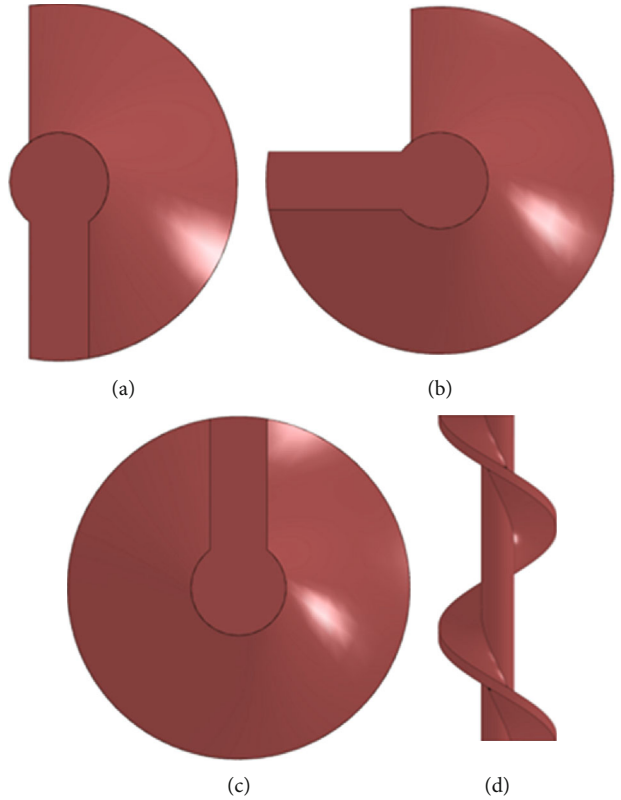

Figure 3: Diagram of impeller with different rotation angles.

The governing equation of the standard k-epsilon model can be expressed in the following general form:

$$\frac{\partial(\rho\phi)}{\partial t}+\frac{\partial(\rho u\phi)}{\partial x}+\frac{\partial(\rho v\phi)}{\partial y}+\frac{\partial(\rho\omega\phi)}{\partial z}=\frac{\partial}{\partial x}\left(\Gamma\frac{\partial\phi}{\partial x}\right)+\frac{\partial}{\partial y}\left(\Gamma\frac{\partial\phi}{\partial y}\right)+\frac{\partial}{\partial z}\left(\Gamma\frac{\partial\phi}{\partial z}\right)+S, \tag{1}$$

where ϕ denotes dependent variable, such as u, v, and ω, Γdenotes the diffusion coefficient, and S denotes the source term of the equation.

In the standard k-epsilon model, the turbulent kinetic energy k and the dissipation rate ε are two basic unknowns, and the corresponding transport equations are as follows:

$$\begin{aligned}\frac{\partial(\rho k)}{\partial t}+\frac{\partial(\rho k u_i)}{\partial x_i}&=\frac{\partial}{\partial x_j}\left[\left(\mu+\frac{\mu_l}{\sigma_k}\right)\frac{\partial k}{\partial x_j}\right]\\&\quad+G_k+G_b-\rho\varepsilon-Y_M+S_k\frac{\partial(\rho\varepsilon)}{\partial t}+\frac{\partial(\rho\varepsilon u_i)}{\partial x_i}\\&=\frac{\partial}{\partial x_j}\left[\left(\mu+\frac{\mu_l}{\sigma_k}\right)\frac{\partial k}{\partial x_j}\right]\\&\quad+C_{1\varepsilon}\frac{\varepsilon}{k}(G_k+C_{3\varepsilon}G_b)-C_{2\varepsilon}\rho\frac{\varepsilon^2}{k}+S_\varepsilon,\end{aligned} \tag{2}$$

where G_k is the generation term of turbulent kinetic energy k caused by average velocity gradient, G_b is the generation term of turbulent kinetic energy k caused by buoyancy, Y_M denotes the contribution of fluctuating expansion in compressible turbulence, $C_{1\varepsilon}$, $C_{2\varepsilon}$, and $C_{3\varepsilon}$ are empirical constants, σ_k and σ_ε are the Prandtl numbers corresponding to the turbulent kinetic energy k and the dissipation rate ε, and S_k and S_ε are the source terms of the equation.

3.2. Boundary Condition. For different nozzles, it is difficult to ensure the same flow rate and pressure drop at the same time. Therefore, the same pressure drop conditions are generally selected for comparative analysis. The nozzle inlet is set as the pressure inlet. The experimental results show that under the condition of 30 MPa pressure difference, the abrasive jet can break most of the rock materials; so, the inlet pressure is set as 30 MPa. The side of the impact external flow field is arranged as a pressure outlet which is atmospheric pressure.

3.3. Discrete Phase Setting. Fluent software provides three multiphase flow models: VOF (volume of fluid) model, mixture model, and Euler model. The Euler model can simulate the multiphase flow of arbitrary composition, and it can also simulate the multiphase flow of interaction [31]. Therefore, the Euler model was selected to study the flow field characteristics of the swirling abrasive jet nozzle. The physical parameters of water can be directly transferred from the Fluent database. The abrasive is set as density 2600 kg/m^3, viscosity 0.0001 kg/m^{-1}, and grain spacing 0.0002. Set the basic phase 1 to water and the phase 2 to abrasive.

3.4. Experimental Project. The impeller is the key component of the swirling abrasive jet nozzle. As shown in Figure 3, its

Table 1: Design of structural parameters of the impeller.

Parameters	Length (mm)	Diameter (mm)	Swirling angle (°)	Blade thickness (mm)	Blade number	Spinning direction
Control group	50	18	360	2.5	3	Clockwise
Swirling angle	50	18	180/270/540	2.5	3	Clockwise
Blade thickness	50	18	360	2/3/3.5/4	3	Clockwise
Blade number	50	18	360	2.5	2/4/5	Clockwise
Swing direction	50	18	360	2.5	3	Counterclockwise

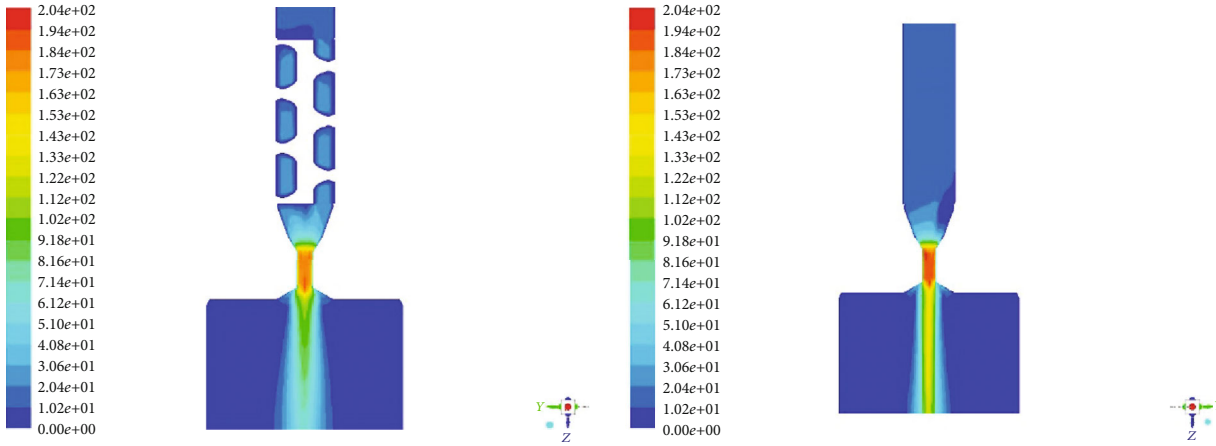

Figure 4: Cloud picture of velocity of swirling abrasive jet and direct jet.

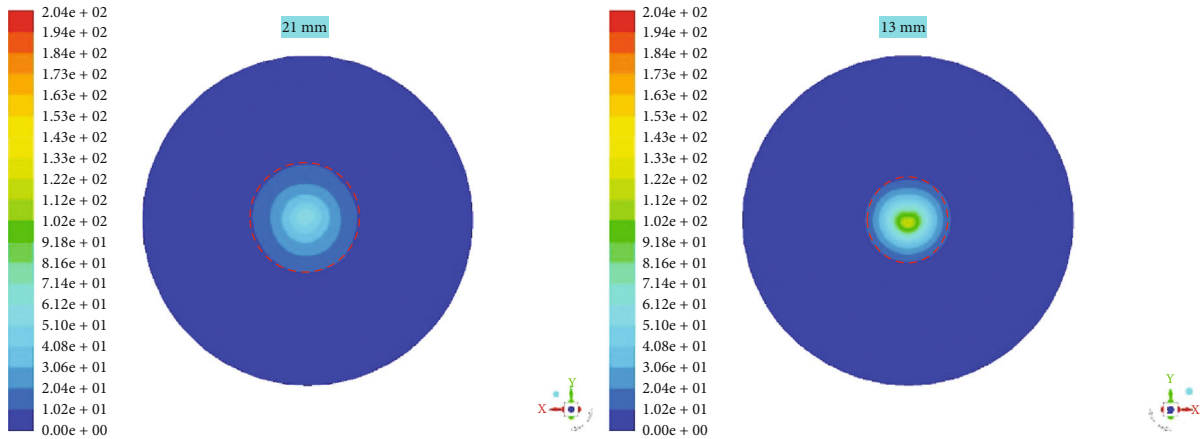

Figure 5: Cloud picture of bottom impact velocity of swirling abrasive jet and direct jet.

key parameters mainly include the following: blade thickness, blade number, blade swirling angle, and spinning direction. The effects of four parameters on the flow field characteristics of the swirling abrasive jet nozzle are studied. In the process of radial horizontal well, the nozzle needs to complete the steering under the steering effect of the deflector. In order to pass the deflector smoothly, the length of the nozzle is generally designed to be 30~50 mm, and the outer diameter is generally 20~30 mm [21, 32–34]. Therefore, the length of the impeller designed in this paper is no more than 50 mm, and the outer diameter is 18 mm. The blade thickness should ensure the strength without occupying too much space, the number of blades should be convenient for processing and occupy less space, and the rotation angle should be considered to cover a larger range during design so as to study its influence rules. The research project is shown in Table 1. Other structural parameters of the swirling abrasive nozzle remain the same.

4. Flow Field Characteristics of the Swirling Abrasive Jet Nozzle

The velocity distribution and impact pressure distribution of the fluid and abrasive particles in the nozzle flow field determine the rock-breaking effect. Specially, the tangential and radial velocity distribution of the swirling jet is of great significance for improving the rock breaking efficiency and forming a large area of rock breaking. In addition, the

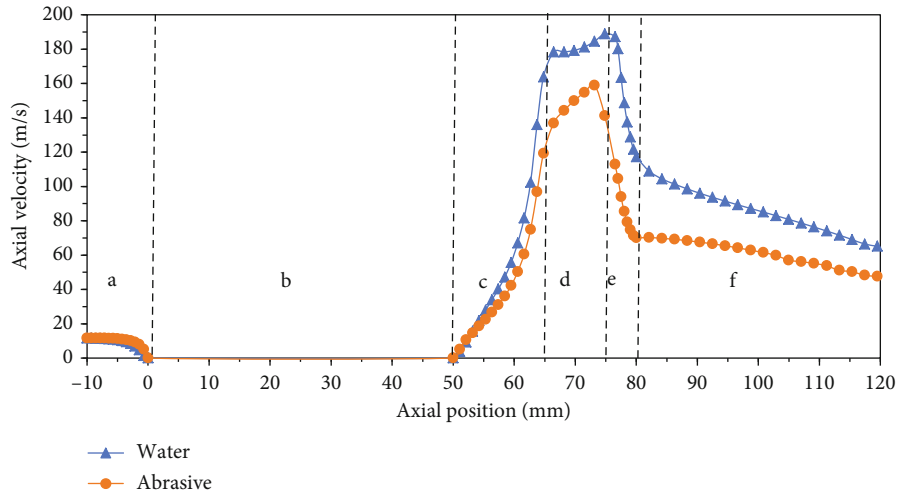

Figure 6: Axial velocity distribution of abrasive and water in swirling abrasive jet (a) inlet section, (b) swirling section, (c) contraction section, (d) cylindrical outlet section, (e) diffusion section, and (f) external flow field section.

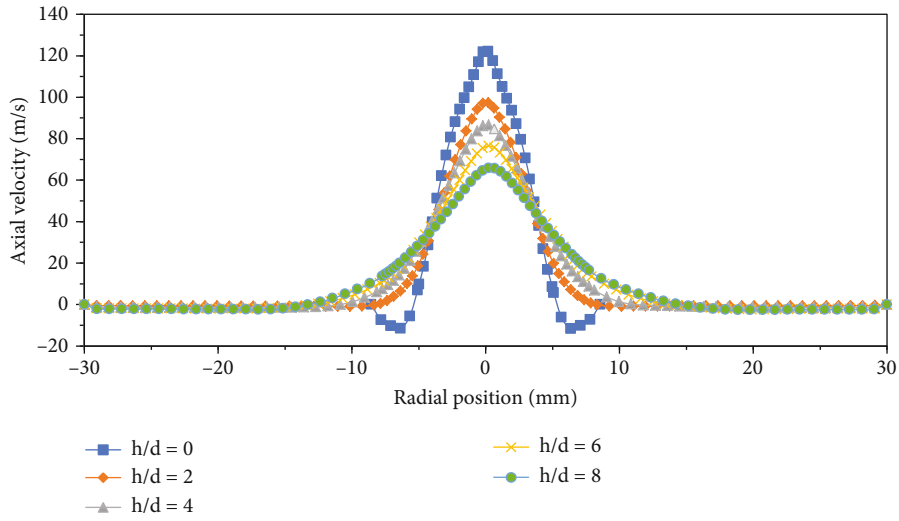

Figure 7: Development law of axial velocity of water.

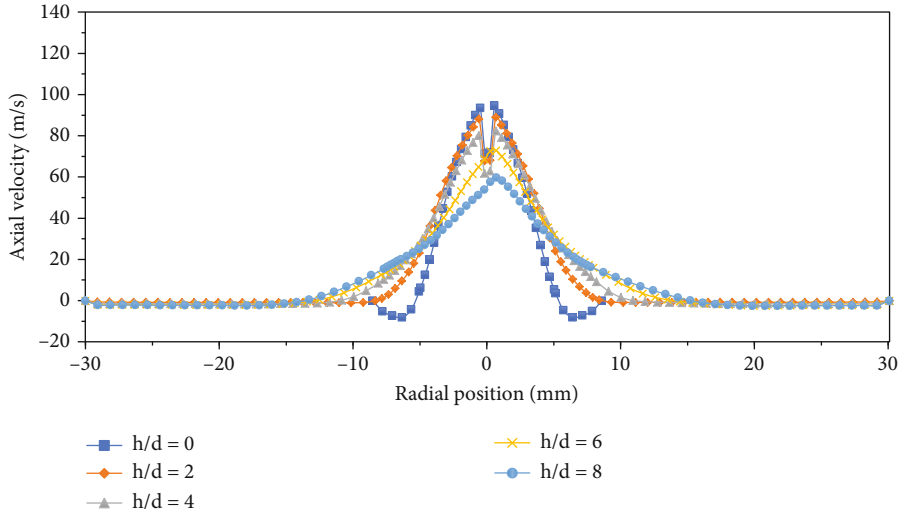

Figure 8: Development law of axial velocity of abrasive.

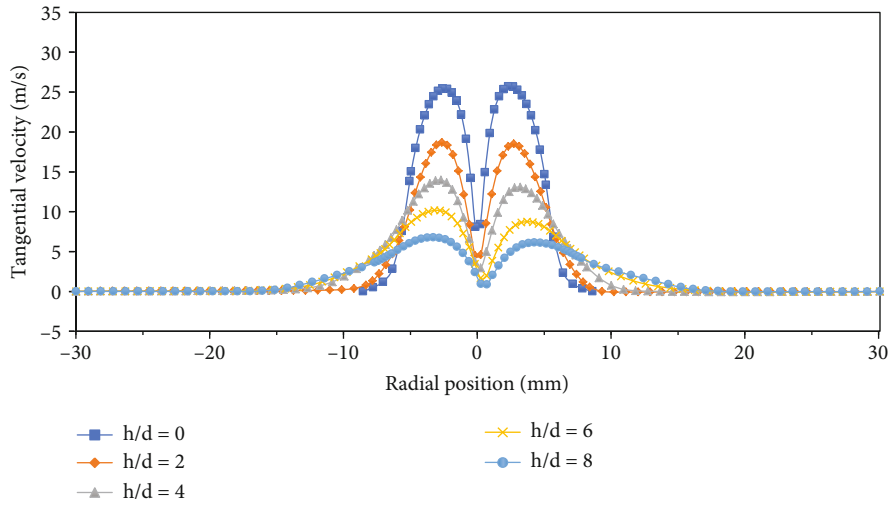

Figure 9: Development law of tangential velocity of water.

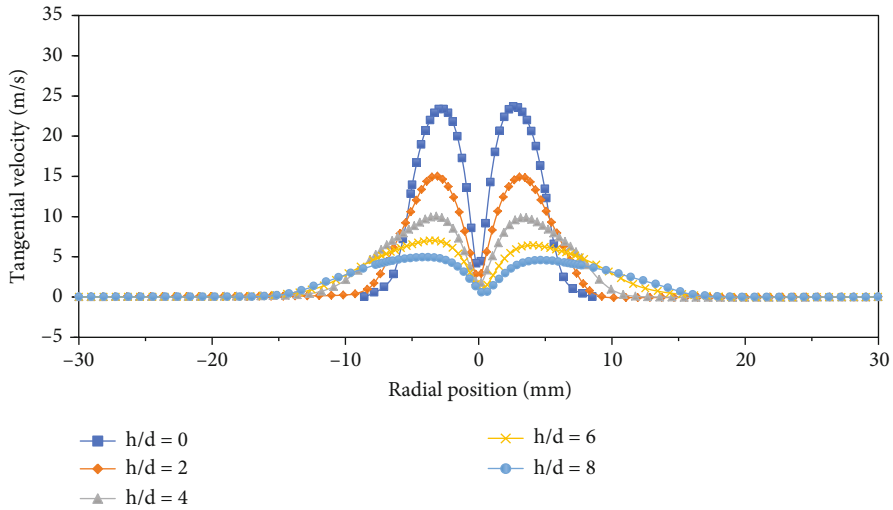

Figure 10: Development law of tangential velocity of abrasive.

rock-breaking ability of abrasive jet is strong, and the velocity distribution characteristics of abrasive particles need to be studied. The flow field of the classical conical nozzle with same equivalent diameter is carried out and compared.

4.1. Flow Field Characteristics of the Swirling Abrasive Jet. The velocity cloud images and jet impact pressure cloud images of the swirling abrasive jet and conical jet are shown in Figures 4 and 5. The flow field structure of swirling abrasive jet nozzle is similar to that of the conical jet, but the swirling abrasive jet has stronger diffusivity; that is, the impact area is larger. Accordingly, the velocity attenuation is fast, the impact pressure is low, and there is no potential core, which is consistent with the research results of Ahmed et al. [34]. It is well known that abrasive jet has high rock breaking efficiency. Therefore, the swirling abrasive jet can effectively break rock and form larger diameter laterals, which is very suitable for RJD technology.

4.2. Axial Velocity Distribution. The axial velocity determines the impact ability of the jet, specially the abrasive needs to obtain sufficient axial velocity to break the rock. The axial velocity of water and abrasive particles is shown in Figure 6. The flow field is divided into six sections from the nozzle inlet: the inlet section (a), the swirling section (b), the contraction section (c), the cylindrical outlet section (d), the diffusion section (e), and external flow field (f). Due to the existence of the impeller, the axial velocity is zero in the swirling section. In the contraction section, the velocity of water increases due to the reduction of the cross-sectional area. The abrasive accelerates under the drag force and pressure difference of water. In the cylindrical outlet section, the velocity of the water is gradually stable, but the velocity of the abrasive is always increasing. In the diffusion section, water and abrasive are ejected from the nozzle, the velocity decreases rapidly due to the loss of the nozzle constraint, and there is no potential core. At the section of the

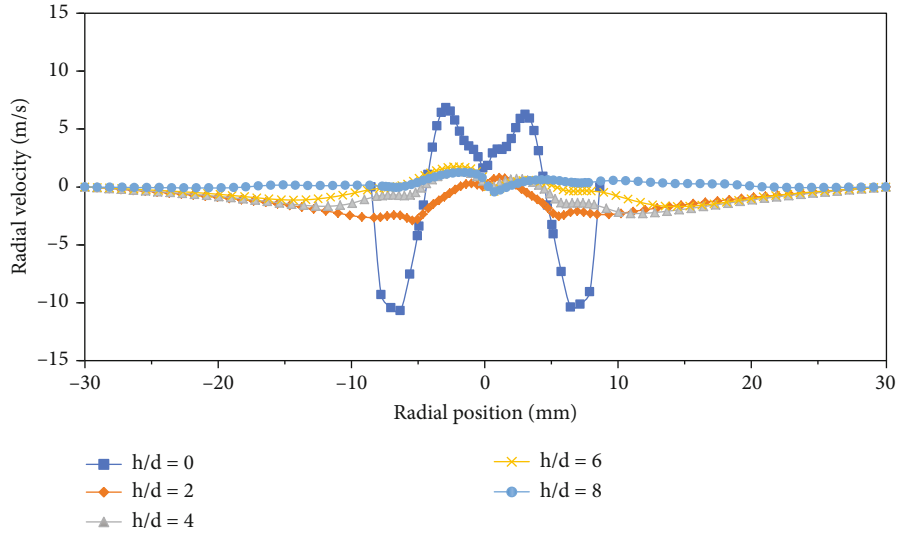

Figure 11: Development of radial velocity of water.

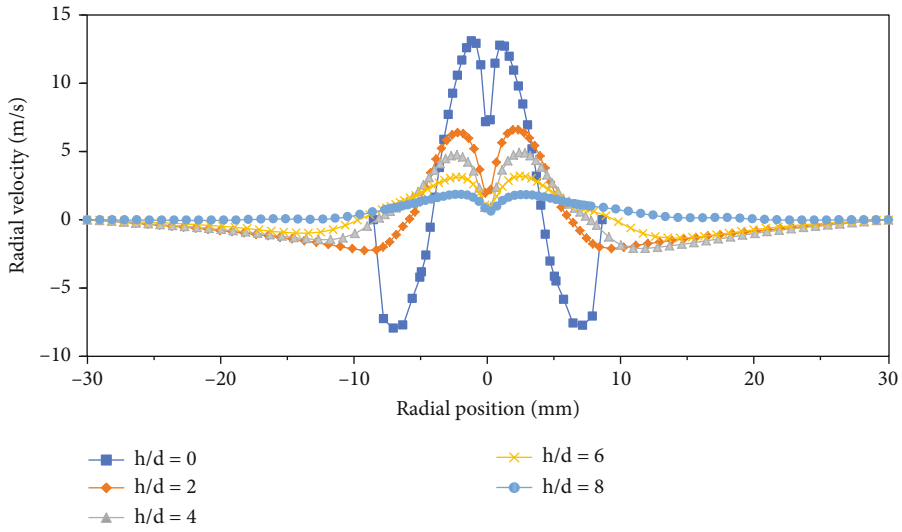

Figure 12: Development of radial velocity of abrasive.

external flow field, the axial velocity begins to decline, but for the speed of the abrasive is still lower than the speed of water, the axial velocity decreasing trend of the abrasive is slower than that of water. After the action of the nozzle, both water and abrasive obtain a higher axial velocity.

4.2.1. Development Law of Axial Velocity. The axial velocity distribution of water and abrasive under different standoff distance is shown in Figures 7 and 8. The zero of the abscissa is set as the center of the nozzle, while the ordinate is the axial velocity. The dimensionless standoff distance (the ratio of the standoff distance to the diameter of the nozzle outlet) is set as 0, 2, 4, 6, and 8. The axial velocity of the swirling abrasive jet obviously has the velocity distribution law of the normal jet, which means that the central velocity is the largest and gradually attenuates along both sides. When the standoff distance is zero, the velocity near the nozzle outlet is negative, which means that entrainment occurs. With the increase of the standoff distance, the jet gradually develops laterally and can form a larger impact area in a certain range. By comparing the axial velocity development curve of abrasive and water, it is found that the velocity of water at the central axis decreases greatly, while the energy loss of abrasive particles is small due to the existence of the speed difference. Therefore, the impact strength of the abrasive can be ensured.

4.3. Development Law of Tangential and Radial Velocity. As we all know, the shear and tensile strength of rock are much lower than its compressive strength, rock is easily broken under the action of shear and tensile stress. Swirling abrasive jet has higher tangential and radial velocity which can produce loads parallel to the surface of the rock, resulting in shear failure. It is necessary to study the development law of tangential velocity and radial velocity.

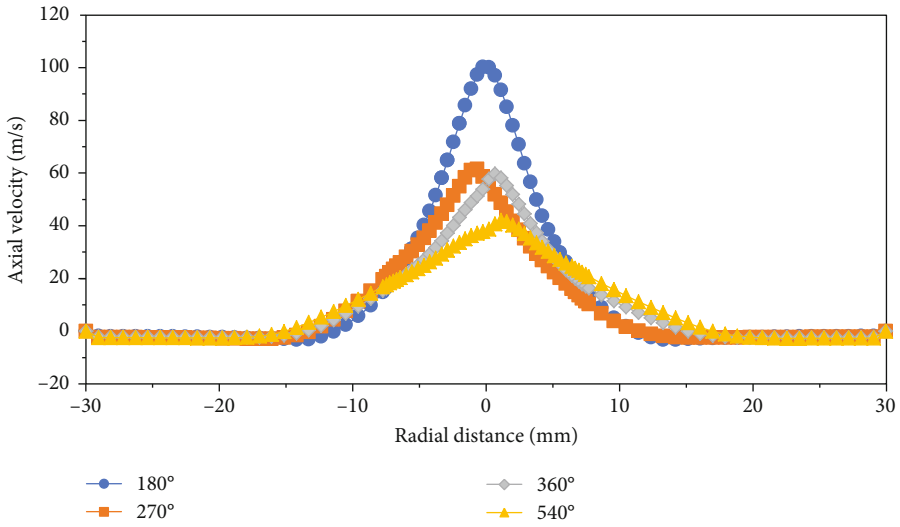

Figure 13: Axial velocity distribution of different spinning angles in $h/d = 8$.

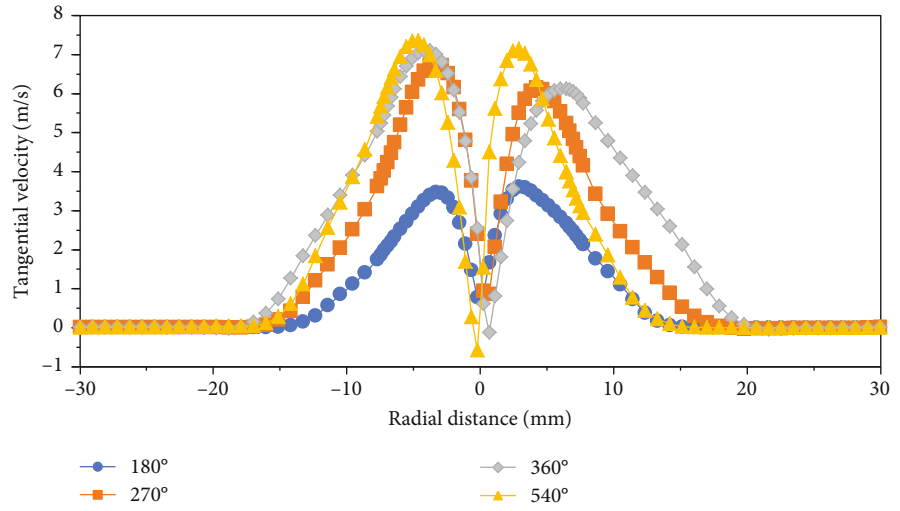

Figure 14: Tangential velocity distribution of different spinning angles in $h/d = 8$.

4.3.1. Distribution Law of Tangential Velocity of Abrasive Particles and Water. Figures 9 and 10 show the distribution of the tangential velocity of water and abrasive particles, the abscissa is the radial distance, and the ordinate is the tangential velocity. The dimensionless standoff distance is set as 0, 2, 4, 6, and 8. Water and abrasive particles do acquire large tangential velocities. The tangential velocity is almost zero along the axis and presents an M-shaped distribution. The maximum tangential velocity will appear at a certain radial radius. At the same time, with the increase of the standoff distance, the maximum tangential velocity gradually develops outward, but the peak value decreases. By comparison, it is found that there is little difference between the tangential velocity of abrasive and that of water, which can improve the efficiency of rock breaking.

4.3.2. Distribution Law of Radial Velocity of Abrasive Particles and Water. Figures 11 and 12 show the distribution of the radial velocity of water and abrasive, the abscissa is the radial radius, and the ordinate is the radial velocity. The dimensionless standoff distance is set as 0, 2, 4, 6, and 8. The radial velocity first increases and then decreases along the radius from the center and shows an symmetrical distribution, which is similar to that of the tangential velocity. When the standoff distance is small, the radial velocity appears negative value, which is due to the influence of entrainment effect. By comparing the radial velocity curve of abrasive and water, it is found that the radial velocity of abrasive particles is larger. However, the radial velocity has a small absolute value and fast attenuation rate. Therefore, radial velocity has little influence on rock breaking, but great influence on impact diameter. However, since the impact diameter can also be obtained from the radial distance where the axial velocity and tangential velocity close to zero, only the axial velocity and tangential velocity are used for analysis in the subsequent analysis.

As mentioned above, water and abrasive in swirling abrasive jet can obtain higher axial, tangential, and radial

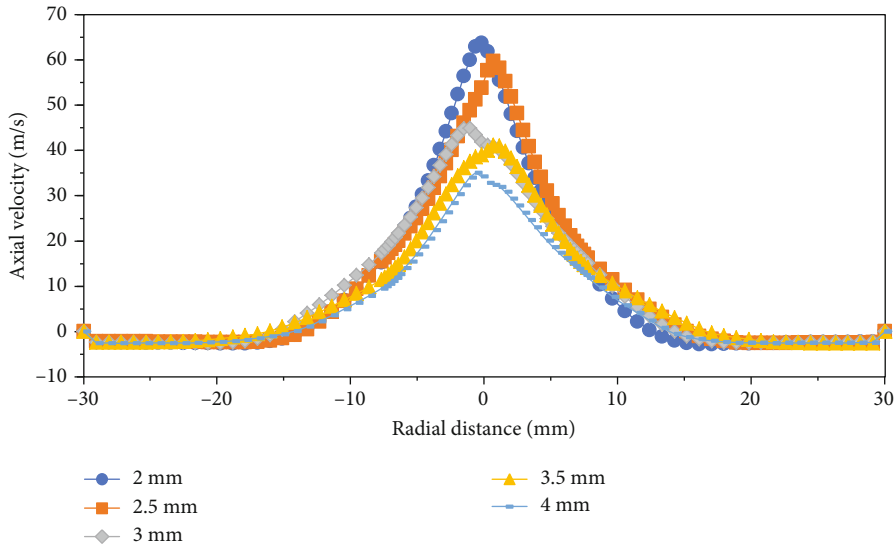

Figure 15: Axial velocity distribution of different blade thickness in $h/d = 8$.

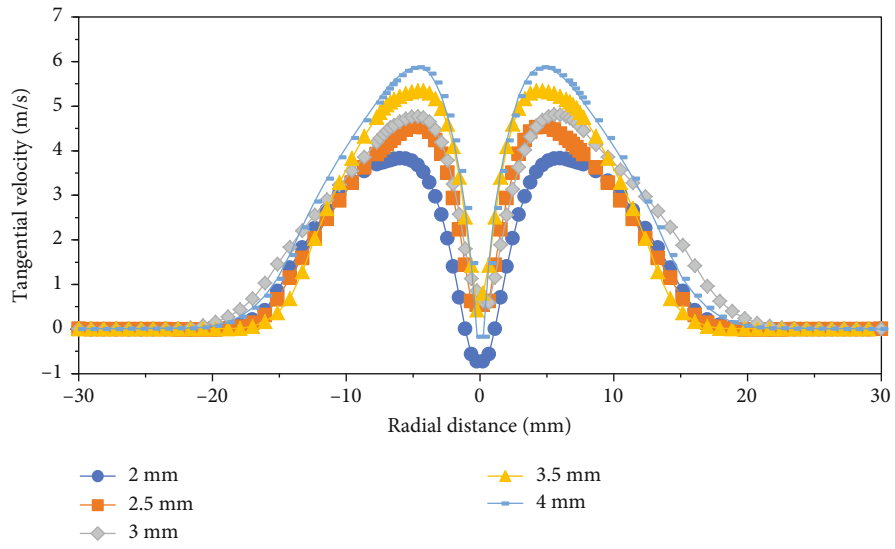

Figure 16: Tangential velocity distribution of different blade thicknesses in $h/d = 8$.

velocities under the guiding of swirling impeller. In other word, the swirling jet velocity is three-dimensional, and its rock breaking manner is mainly of slopping impact, which make it high rock breaking efficiency [35]. The tangential velocity presents an M-shaped distribution, and its maximum value appears on a ring at a certain distance from the jet center, which explains the phenomenon that rock fragmentation by swirling jet will form a circular region [36]. The radial velocity distribution shows the phenomenon of entrainment, but its absolute value is small and is not considered in the follow-up study.

5. Influence of Structural Parameters

In order to perform radial drilling well, the nozzle should simultaneously achieve high efficiency rock breaking and large diameter hole-forming [37]. According to the above analysis, the axial velocity and tangential velocity determines the rock-breaking efficiency. The core part of the swirling abrasive jet nozzle is the impeller. Therefore, the influence of various parameters of the impeller on the axial and tangential velocity is mainly analyzed.

5.1. Influence of Swirling Angle of Impeller. When the diameter and length of the impeller are constant, the swirling angle of the impeller determines the rotation of the fluid. The initial rotation angle is positioned at 180 degrees, followed by an increase of 90 degrees. In order to study the influence of a larger range of angles, the last group is positioned at 540°. To evaluate the impact effect, the axial and tangential velocities near the impact plane where the dimensionless standoff distance is equal to 8 are selected for analysis. As shown in Figures 13 and 14, with the increase of rotation angle, the axial velocity distribution becomes smoother, and the peak value

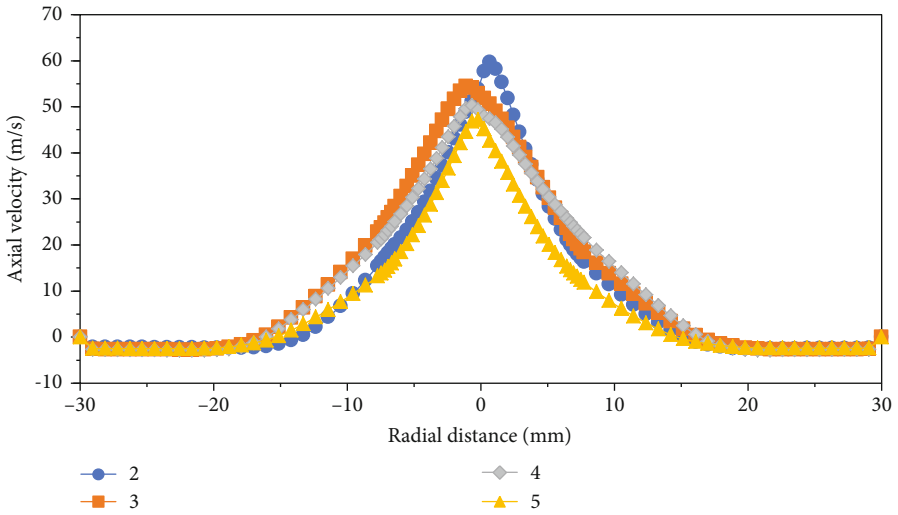

Figure 17: Axial velocity distribution of different blade thicknesses in $h/d = 8$.

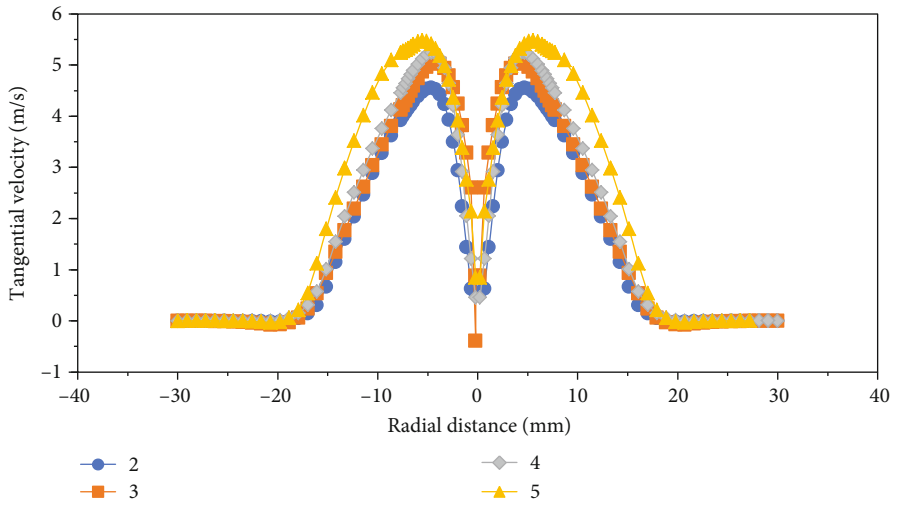

Figure 18: Tangential velocity distribution of different blade thicknesses in $h/d = 8$.

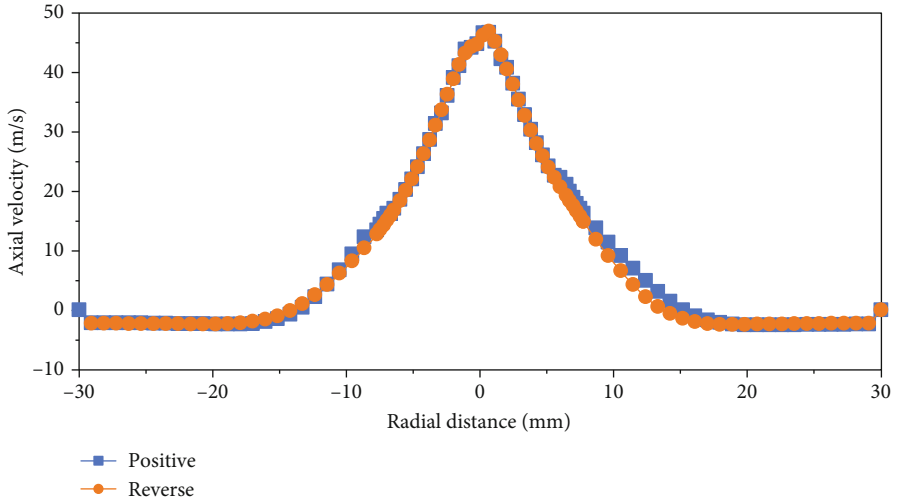

Figure 19: Axial velocity distribution of positive and reverse swirling in $h/d = 8$.

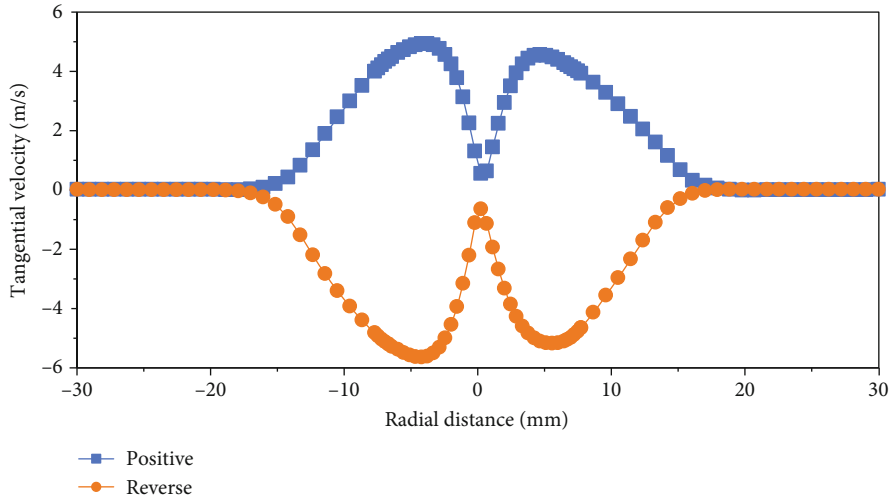

Figure 20: Tangential velocity distribution of positive and reverse swirling in $h/d = 8$.

decreases, while the peak tangential velocity gradually increases. It can be seen that with the increase of rotation angle, abrasive and fluid can obtain more tangential velocity, which can promote rock failure by shear action. When the rotation angle is greater than 270°, the influence of the rotation angle on the axial and tangential velocities decreases. Therefore, under the condition of this paper, the rotation angle is recommended to be no less than 270°.

5.2. Influence of Blade Thickness. When the other parameters of the impeller are constant, the impeller thickness affects the flow section and then the rotation capacity. The influence of the blade thickness on the abrasive flow field is carried out. Figures 15 and 16 show the axial and tangential velocity distributions of abrasive particles when the dimensionless standoff distance is 8 and the blade thickness is 2 mm, 2.5 mm, 3 mm, 3.5 mm, and 4 mm. It can be seen from Figure 16 that the tangential velocity of abrasive gradually increases with the increase of blade thickness, and the peak value of blade thickness 4 mm is the highest; so, it is recommended to increase blade thickness. Correspondingly, as shown in Figure 15, the axial velocity decreases with the increase of blade thickness. Although increasing the blade thickness can increase the tangential velocity, the increase is small and will lead to the increase of flow resistance. Therefore, 2.5 mm is recommended under the conditions of this paper.

5.3. Influence of Blade Number. The influence of the number of blades on the flow field of abrasive is carried out. Figures 17 and 18 show the axial and tangential velocity distributions of abrasive particles when the dimensionless standoff distance is 8 and the number of blades is 2, 3, 4, and 5. With the increase of the number of blades, the peak axial velocity decreases slightly while the tangential velocity increases. Generally, the number of blades has little effect. Considering axial velocity and tangential velocity, the recommended number of blades is 3.

5.4. Influence of the Spinning Direction. The influence of the swirling direction of impeller on the abrasive flow field is also studied. Figures 19 and 20 show the axial and tangential velocity distributions of abrasive particles when the dimensionless standoff distance is 8. It can be seen from Figures 18 and 19 that the axial velocities basically are the same while tangential velocities are mirrored, which means their absolute values, the development law, and expansion range are basically the same. Therefore, the spinning direction will not affect the flow field of the swirling abrasive jet.

6. Conclusion

Swirling abrasive jet technology can realize large diameter and efficient rock-breaking and hole-forming, which can greatly promote the development RJD technology. In order to better understand its working principle and improve its performance, the flow field characteristics and key impeller parameters of swirling abrasive jet nozzles are studied by numerical simulation, and the main conclusions are as follows:

(1) Compared with the direct jet, the flow field structure of the swirling abrasive jet is basically the same, but it has no constant velocity core, and its diffusivity is stronger, which can form a larger impact area; that is, the swirling abrasive jet nozzle can form a larger diameter rock-breaking

(2) Under the action of swirling impeller, abrasive particles can obtain larger axial and tangential velocities. The velocity of abrasive particles increases with the velocity of water, and when it comes out of the nozzle, the velocity of abrasive particles attenuates slowly. The tangential velocity shows an "M" distribution along the radial direction of the nozzle, which has a low central velocity and a high surrounding velocity. The radial velocity shows that there is an entrainment region. The combination of axial, tangential, and radial velocities can better break the rock by tensile shear, form a larger rock-breaking diameter, and improve the efficiency

(3) With the increase of the spinning angle, the axial velocity of the fluid decreases, and the tangential velocity increases gradually. With the increase of blade thickness, the axial velocity decreases, and the tangential velocity increases gradually. With the increase of the number of blades, the axial velocity decreases, and the tangential velocity increases gradually. The spinning direction almost has no effect on the flow field. Therefore, the spinning angle is recommended to be no less than 270°, blade thickness is 2.5 mm, and number of blades are 3

Data Availability

When data is required, the corresponding author can be contacted.

Conflicts of Interest

The authors declare that they have no conflicts of interest.

Acknowledgments

This support is gratefully acknowledged by the authors, who are also grateful to the reviewers of this paper for their detailed comments. This study was supported by the Foundation of State Key Laboratory of Shale Oil and Gas Enrichment Mechanisms and Effective Development (No. 35800000-20-ZC0609-0006), National Key Research and Development Program (2019YFB1504202), and Science Foundation of China University of Petroleum, Beijing (No. 2462021YJRC009).

References

[1] W. Dickinson and R. W. Dickinson, "Horizontal radial drilling system," in *The SPE California Regional Meeting, Conference*, pp. 27–29, Bakersfield, California, 1985.

[2] W. Dickinson, R. R. Anderson, and R. W. Dickinson, "The ultrashort-radius radial system," *SPE Drilling Engineering*, vol. 4, no. 3, pp. 247–254, 1989.

[3] LANDERS C W, *Method of and apparatus for horizontal well drilling: US Patent No. 5853056*, 1998.

[4] B. Marbun and S. Putra, "Review of ultrashort-radius radial system (URRS)," in *Proceedings of the international petroleum technology conference*, Bangkok, 2011.

[5] R. A. Cirigliano and J. F. T. Blacutt, "First experience in the application of radial perforation technology in deep wells," in *Latin American & Caribbean Petroleum Engineering Conference*, Buenos Aires, Argentina, 2007.

[6] M. K. Medetbekova, S. Salimzadeh, H. F. Christensen, and H. M. Nick, "Experimental and numerical study of the stability of radially jet drilled laterals in chalk reservoirs," in *80th EAGE conference and exhibition 2018*, Copenhagen, 2018.

[7] S. D. Cinelli and A. H. Kamel, "Novel technique to drill horizontal laterals revitalizes aging field," in *SPE/IADC Drilling Conference*, Amsterdam, The Netherlands, 2013.

[8] Q. Liu, S. Tian, G. Li et al., "An analytical model for fracture initiation from radial lateral borehole," *Journal of Petroleum Science and Engineering*, vol. 164, pp. 206–218, 2018.

[9] Y. Wang, B. Hou, W. Dong, and Z. Jia, "Features of fracture height propagation in cross-layer fracturing of shale oil reservoirs," *Petroleum Exploration and Development*, vol. 48, no. 2, pp. 469–479, 2021.

[10] B. Hou, Y. Dai, C. Zhou, K. Zhang, and F. Liu, "Mechanism study on steering acid fracture initiation and propagation under different engineering geological conditions," *Geomechanics and Geophysics for Geo-Energy and Geo-Resources*, vol. 7, no. 3, pp. 1–14, 2021.

[11] K. Zhang, B. Hou, M. Chen, C. Zhou, and F. Liu, "Fatigue acid fracturing: a method to stimulate highly deviated and horizontal wells in limestone formation," *Journal of petroleum science and engineering*, vol. 208, p. 109409, 2022.

[12] Q. Zhang, B. Hou, B. Lin, X. Liu, and Y. Gao, "Integration of discrete fracture reconstruction and dual porosity/dual permeability models for gas production analysis in a deformable fractured shale reservoir," *Journal of Natural Gas Science and Engineering*, vol. 93, p. 104028, 2021.

[13] X. Li and J. He, "Research and application of radial borehole fracturing based on numerical simulation," *Geofluids*, vol. 2019, 16 pages, 2019.

[14] T. Reinsch and D. Bruhn, "The SURE consortium (2016) Novel productivity enhancement concept for a sustainable utilization of a geothermal resource e the SURE project," in *In: Proceedings, European geothermal Congress 2016*, Strasbourg, 2016.

[15] Y. Shi, X. Song, G. Wang, J. Li, L. Geng, and X. Li, "Numerical study on heat extraction performance of a multilateral-well enhanced geothermal system considering complex hydraulic and natural fractures," *Renewable Energy*, vol. 141, pp. 950–963, 2019.

[16] Y. Q. Zhang, K. X. Zhao, X. Y. Wu et al., "An innovative experimental apparatus for the analysis of natural gas hydrate erosion process using cavitating jet," *The Review of Scientific Instruments*, vol. 91, no. 9, article 095107, 2020.

[17] Y. Zhang, X. Wu, X. Hu et al., "Visualization and investigation of the erosion process for natural gas hydrate using water jet through experiments and simulation," *Energy Reports*, vol. 8, pp. 202–216, 2022.

[18] Z. L. Ge, K. Deng, Z. Zhou, M. Yang, and C. Chai, "Fracture characteristics of coal jointly impacted by multiple jets," *Engineering Fracture Mechanics*, vol. 235, p. 107171, 2020.

[19] L. Jingbin, H. Zhongwei, Z. Guangqing, L. Xin, and L. Huan, "Rock breaking characteristics of the self-rotating multi-orifices nozzle applied to coalbed methane radial jet drilling," *International Journal of Rock Mechanics and Mining Sciences*, vol. 136, p. 104483, 2020.

[20] C. Dong, Y. Li, J. Long, Q. Zhang, D. Wang, and J. Wu, "Operation optimization of plugged screen cleanup by rotary water jetting," *Petroleum Science*, vol. 11, no. 1, pp. 122–130, 2014.

[21] H. Liao, D. Wu, L. Wang, and L. Zhu, "Comparisons of spraying structure and rock breakage characteristics of round straight, swirling, and straight-swirling integrated jets," *Atomization and Sprays*, vol. 23, no. 4, pp. 363–377, 2013.

[22] A. W. Momber and R. Kovacevic, "test parameter analysis in abrasive water jet cutting of rocklike materials," *International Journal of Rock Mechanics and Mining Sciences*, vol. 34, no. 1, pp. 17–25, 1997.

[23] Y. Liu, J. Zhang, T. Zhang, and H. D. Zhang, "Optimal nozzle structure for an abrasive gas jet for rock breakage," *GEOFLUIDS*, vol. 2018, 14 pages, 2018.

[24] W. Zuo, C. Huang, Y. Liu et al., "Analysis and modeling of particle velocities in premixed abrasive water jets," *GEOFLUIDS*, vol. 2020, 9 pages, 2020.

[25] J. B. Surjaatmadja, S. R. Grundmann, and B. McDaniel, "Hydrajet fracturing: an effective method for placing many fractures in openhole horizontal wells," Proceedings of, Society of Petroleum Engineers, 1998.

[26] L. I. Gensheng, H. U. A. N. G. Zhongwei, and T. I. A. N. Shouceng, "Research and application of water jet technology in well completion and stimulation in China," *Petroleum Science*, vol. 7, no. 2, pp. 239–244, 2010.

[27] Z. H. Zhu, T. Feng, Z. G. Yuan, D. H. Xie, and W. Chen, "Solid-gas coupling model for coal-rock mass deformation and pressure relief gas flow in protection layer mining," *Advances in Civil Engineering*, vol. 2018, 6 pages, 2018.

[28] Z. Huang, J. Niu, G. Li, X. Yuan, and Y. Liu, "Surface experiment of abrasive water jet perforation," *Petroleum Science & Technology*, vol. 26, no. 6, pp. 726–733, 2008.

[29] J. Niu, G. Li, and J. Song, "An experimental study on abrasive water jet perforation parameters," *PETROLEUM DRILLING TECHNIQUES*, vol. 31, no. 2, pp. 14–16, 2003.

[30] Y. Yang, Z. Shen, and R. Wang, "Experimental study on rotary abrasive jet drilling," *PETROLEUM DRILLING TECHNIQUES*, vol. 27, no. 4, pp. 4–6, 1999.

[31] B. Yuhuan, R. Wang, and Z. Weidong, "Study on the law of rock breaking and hole formation by rotating jet," *Journal of rock mechanics and engineering*, vol. 22, no. 4, pp. 664–668, 2004.

[32] Y. Liu, Q. Ba, L. He, K. Shen, and W. Xiong, "Study on the rock-breaking effect of water jets generated by self-rotatory multinozzle drilling bit," *Energy Science and Engineering*, vol. 8, no. 7, pp. 2457–2470, 2020.

[33] R. S. Balch, T. Ruan, and M. Savage, "Field testing and validation of a mechanical alternative to radial jet drilling for improving recovery in mature oil wells," Society of Petroleum Engineers, 2016.

[34] Z. U. Ahmed, Y. M. Al-Abdeli, and F. G. Guzzomi, "Impingement pressure characteristics of swirling and non-swirling turbulent jets," *Experimental Thermal and Fluid Science*, vol. 68, pp. 722–732, 2015.

[35] N. Hongjian and R. Wang, "A study of the rock breaking mechanism during swirling water jet drilling," *Petroleum Science*, vol. 1, no. 1, pp. 39–44, 2004.

[36] R. Wang and N. Hongjian, "Numerical analysis on rock-breaking mechanism using swirling water jet," *Journal of the University of Petroleum China*, vol. 27, no. 1, pp. 33–35, 2003.

[37] J. Li, J. Dai, Z. Huang, G. Zhang, X. Liu, and H. Li, "Rock breaking characteristics of the self-rotating multi-orifice nozzle for sandstone radial jet drilling," *Rock Mechanics and Rock Engineering*, vol. 54, no. 11, pp. 5603–5615, 2021.